Colloids and Surfaces A: Physicochemical and Engineering Aspects 674 (2023) 131885

Contents lists available at ScienceDirect

Colloids and Surfaces A: Physicochemical and Engineering Aspects

journal homepage: www.elsevier.com/locate/colsurfa

Dip coating of viscous granular suspensions

Connor Copeland, Chase T. Gabbard, Joshua B. Bostwick *

Department of Mechanical Engineering, Clemson University, Clemson, SC, 29634, USA

HIGHLIGHTS

- Dip coating of particle suspensions can be used as a method for particle filtration of monodisperse suspensions.
- Particle sorting of bidisperse suspensions can be achieved for a range of capillary numbers.
- Performed experiments over a wide range of experimental conditions including granular particles and highly viscous liquids, thus extending and validating prior work on capillary particle filtration.

GRAPHICAL ABSTRACT

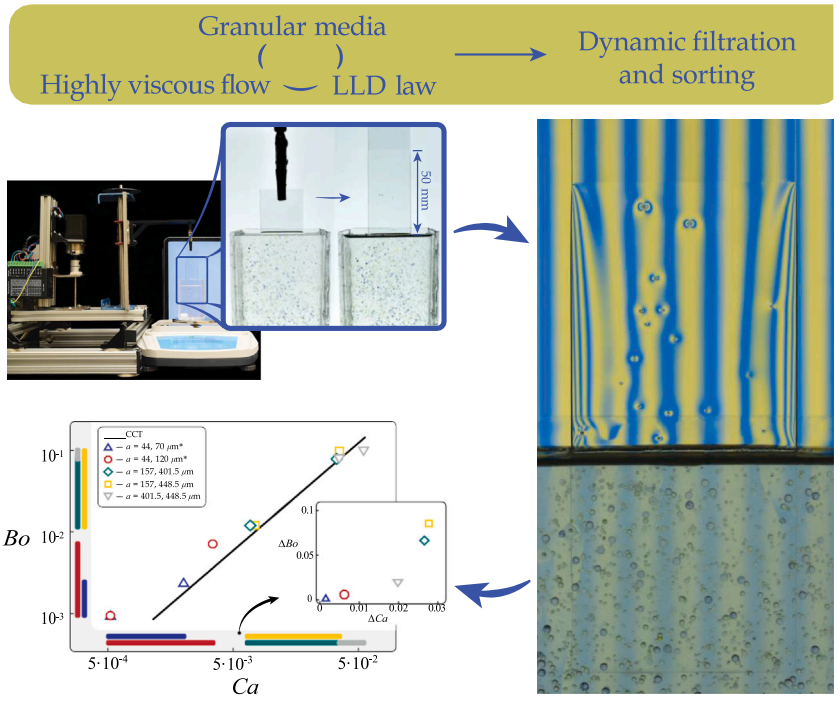

ARTICLE INFO

MSC:
76A20
76D45
76T20

Keywords:
Particle filtration
Suspensions
Thin film flows

ABSTRACT

A solid substrate withdrawn from a liquid bath is coated with a uniform thickness given by the Landau–Levich–Derjaguin (LLD) law. If the bath is a suspension of neutrally buoyant particles, the liquid coating can entrain particles in a process known as capillary filtration that only depends on the capillary number Ca. Experiments were performed using a custom-built dip coating apparatus and gravimetry techniques. The working liquids were monodisperse and bidisperse suspensions with larger particle diameters and higher liquid viscosity than previously reported. The single particle entrainment point for monodisperse suspensions agrees well with the critical capillary number predicted in prior literature. Bidisperse suspensions exhibit active filtration regions where only the smallest particles are entrained with the range of Ca for active filtration consistent with

* Corresponding author.
E-mail address: jbostwi@clemson.edu (J.B. Bostwick).

https://doi.org/10.1016/j.colsurfa.2023.131885
Received 20 April 2023; Received in revised form 12 June 2023; Accepted 13 June 2023
Available online 20 June 2023

Surface tension

reported models. These experimental results both validate and enhance our understanding of capillary filtration by exploring larger particle-sized granular suspensions of higher viscosity solutions, as relevant to applications in construction, medical care, personal care products, and food science.

1. Introduction

Dip-coating is a common coating technique where a substrate is slowly removed from a liquid bath, resulting in a thin coating. This process has numerous applications, including photographic film fabrication, fiber optic cable coating, and general coating processes [1–4]. These applications often use coatings with complex structures, such as liquids with suspended particulate matter, to enhance their functionality. Moreover, particulate suspensions are commonly encountered in a wide range of manufacturing, biomedical, and industrial applications, as well as in geophysical flows [5–7]. The ubiquitous presence of suspensions in nature and industry and the frequent use of dip coating in manufacturing have motivated a recent demand for further fundamental research into the physics of dip coating of granular suspensions.

A typical dip-coating process using a particle suspension is shown in Fig. 1(*a*). The bath is considered a suspension because the particles' gravity-induced displacement, which depends upon the gravity F_g and buoyancy F_b acting on the particle, is negligible compared to plate displacement during dip coating. Sauret et al. [8] pioneered the current surge in the literature on such systems by testing monodisperse suspensions over a wide range of substrate velocities U. They found that small particulate matter can become entrained in the liquid coating and removed from the bath via 'capillary filtration'. Dincau et al. [6] built upon the idea of capillary filtration by showing that dip coating of bidisperse suspensions can sort particles of different sizes by entraining small particles in the coating and leaving large particles in the bath over a certain range of substrate velocities. Thus, dip coating shows promise as a novel filtering and sorting process that is scalable, resistant to clogging or degradation, and tunable, addressing many of the limitations plaguing current filtration techniques [5,6,9]. Here, we build upon these works by conducting experiments for larger particles in the granular range and highly viscous liquids allowing us to explore capillary numbers and Bond numbers not yet studied in experiments.

In 1942, Levich and Landau [1] proposed the first model describing the coating thickness of a substrate removed from a completely-wetting, Newtonian liquid. Their seminal work was later expanded on by Derjaguin [10], resulting in the well-known Landau–Levich–Derjaguin (LLD) law

$$h_0 = 0.945\ell_c Ca^{2/3}, \tag{1}$$

where h_0 is the coating thickness, $\ell_c \equiv \sqrt{\sigma/\rho g}$ is the capillary length, and $Ca = \mu U/\sigma$ is the capillary number, which compares viscous to capillary forces. Thus, dip coating depends upon the substrate's withdrawal velocity U, gravity g, and the liquid's properties: dynamic viscosity μ, surface tension σ, and density ρ.

Eq. (1) highlights the crucial role of Ca in tuning the coating thickness h_0. When $Ca < 10^{-3}$, the flow regime is visco-capillary but when $Ca > 1$ it is visco-gravitational [10,11]. This interplay of forces is also responsible for the shape of the meniscus [11–13]. The region between the visco-capillary and visco-gravitational regime is quite broad and a unifying theory was derived by Tallmadge [14] through matching of the profile $h(x)$ first proposed by Landau [1,14] and later corrected by Spiers et al. [15]. Notably, when liquids only partially wet the substrate, surfactant can improve their wettability. However, many studies have shown that surfactants can also lead to thicker films than those predicted by Eq. (1) [16–19].

Sauret et al. [8] showed that single particles can be filtered from a monodisperse suspension, which Colosqui et al. [7] hypothesized was dependent upon the stagnation point S^* with width h^*. The stagnation point and corresponding thickness are illustrated in Fig. 1(*a*) and h^* can be determined using

$$\frac{h^*}{l_c} = 3\left(\frac{h_0}{l_c}\right) - \frac{\left(\frac{h_0}{l_c}\right)^3}{Ca}. \tag{2}$$

Colosqui et al. [7] determined the critical thickness for particle entrainment is $2a > h^*$ based on their simulations for $Ca < 10^{-2}$. The Bond number $Bo = (a/l_c)^2$ gives the particle diameter in a nondimensional form; thus, the entrainment threshold in terms of the critical capillary number Ca^* is

$$Ca^* = DBo^{3/4} \tag{3}$$

where the prefactor D was found to be $D = 0.59$ by Colosqui et al. [7] for single particle entrainment for $Ca > Ca^*$. Dincau et al. [6] later found that $D = 0.24$ best fit their empirical data. The capillary force responsible for entrainment increases for clumps of particles, allowing for particle clumps to be entrained for $Ca < Ca^*$ [6,8,20]. Fig. 1(*b*) shows images of the three entrainment regimes for monodisperse suspensions: (i) liquid only, (ii) clumps, and (iii) single particle entrainment. Particle entrainment is not limited to planar substrates [21–23] and can be induced by the flow of a bubble in a capillary tube [24], further increasing its versatility as a filtration method.

The relationship between Bo and Ca^* suggests that a bidisperse suspension will have two Ca^*. Dincau et al. [6] demonstrated this by showing an 'active filtration' range where only the small particles were entrained. The lower three images of Fig. 1(*b*) show examples of the liquid-only, active filtration, and all-particle entrainment observed as Ca increases. The values of each Ca^* and the range of active filtration can be calculated using the critical capillary number introduced by Colosqui et al. [7] using

$$\Delta Ca = Ca_B^* - Ca_S^* = 0.24\left(\frac{a_B}{l_c}\right)^{3/2}\left(1 - \left(\frac{a_S}{a_B}\right)^{3/2}\right), \tag{4}$$

where a_B and a_S are the average radius of the big and small particles, respectively. More recently, Jeong et al. [25] experimentally explored dip coating of bidisperse suspensions for particles with $a \leq 125$ μm and found that the composition of the coating film evolves with the withdrawal velocity.

Dip coating is a versatile method for filtering and sorting particles from a liquid bath. Previous research has focused on small particulate ($2a \leq 240$ μm) suspended in a single viscosity $\mu = 132$ mPa · s solution [6]. Here, we expand the parameter space to include larger granular-sized particulate and higher viscosity liquids, as relevant to applications in construction, medical care, food production, personal care products, smart coatings, and environmental flows. For example, granular microspheres ($2a > 100$ μm) in injectable suspensions and gels are commonly used for medical care such as drug delivery, embolization therapies, as a filler and bulking agent, and in bone regeneration cement [26,27]. In all of these applications, a tunable particle filtration method would give precise control over the particle size distribution and concentration to tailor the mechanical properties of the injection. In addition, many common culinary products require knowledge of how granular media interact with a highly viscous flow. Examples include

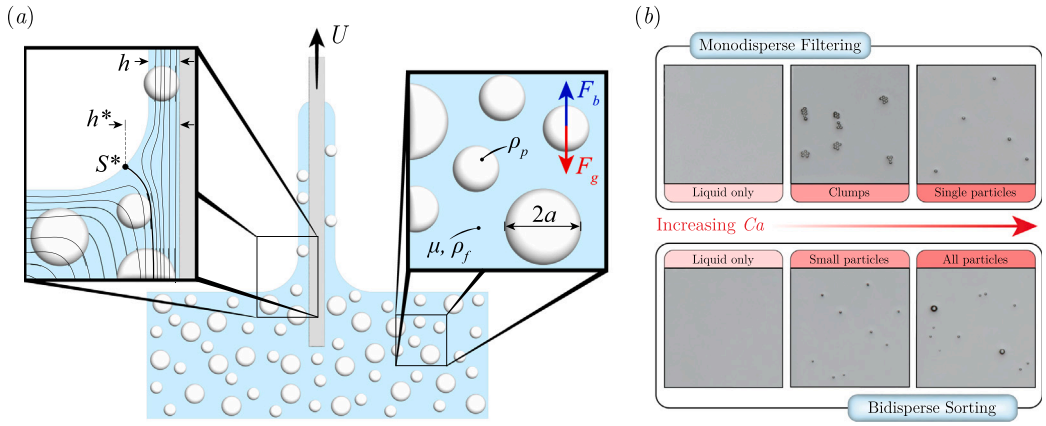

Fig. 1. (*a*) Schematic of the dip coating processes for a bidisperse suspension. The magnified regions show the critical features of the meniscus for particle entrainment (left) and the relevant particle and liquid properties of the suspension (right). (*b*) Typical images of a glass slide withdrawn from a monodisperse (top) and bidisperse (bottom) suspension showing filtering of a monodisperse suspension and sorting of a bidisperse suspension, as capillary number Ca increases.

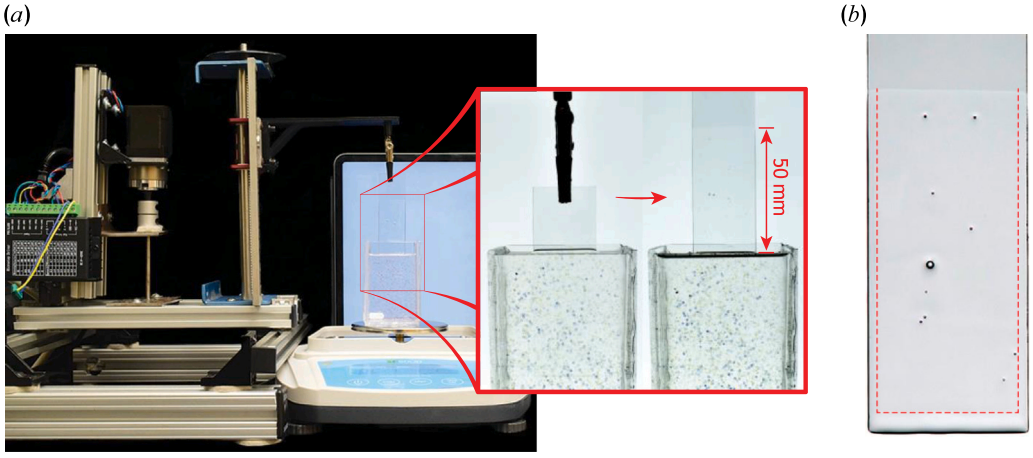

Fig. 2. (*a*) Experimental apparatus with blow-up of the testing region showing initial and final positions of the substrate. (*b*) Typical image of a glass substrate showing entrained particles within the region of constant film thickness (red, dashed line).

filtering propolis remains from highly viscous honey, ensuring the correct particle sizes in crunchy ($2a > 1.59$ mm) and creamy ($2a < 1.59$ mm) peanut butter [28], and coating sweets with chocolate and caramel—which often contain small granular pieces for enhanced flavor. Beyond the kitchen, viscous-granular suspensions are abundant in personal care products including facial creams and body lotions, which are highly viscous [29–31] and typically contain suspended exfoliating particles with diameters up to $2a = 425$ μm [32].

The examples above illustrate the relevance of highly viscous granular suspensions in our everyday life and highlight the need to develop effective methods for controlling the particle size distribution. Here, we present an experimental study to address this need by expanding the literature on particle sorting and particle filtration to higher viscosity liquids and larger particle diameters. We describe our experiment in Section 2, and our findings for liquid-only dip coating, monodisperse suspensions, and bidisperse suspensions in Sections 3.1, 3.2, and 3.3, respectively. Section 4 discusses our results and potential avenues for further exploration, and Section 5 states our conclusions.

2. Experiment

Experiments were performed using the setup shown in Fig. 2(*a*). The dip coating apparatus was built in-house and uses a linear actuator, Arduino-controlled stepper motor, a microstep driver, and vibration dampeners to produce smooth and precise substrate motion. Clean glass slides (75 × 26 mm) are used as the substrate and were imaged using a DSLR camera and a white backlight for contrast. In each experiment, the glass slide is lowered 50 mm into the bath, and then raised 50 mm at a constant velocity U as shown in the magnified region of Fig. 2(*a*). During the experiment, the liquid container remains on an analytical scale (0.001 g), allowing us to use gravimetry analysis to determine the film thickness h_0. We note that although the dip-coated film is mostly uniform, the film becomes nonuniform near the vertical edges and bottom edge [33]. In this study, we ignore these edge effects by only considering the film thickness and particle entrainment in the uniform region shown by the dashed red line in Fig. 2(*b*).

Three sets of experiments were performed with the following working liquids; (i) pure liquid, (ii) monodisperse suspensions, and (iii) bidisperse suspensions. Silicone oils were used for all experiments since they fully wet the substrate and are available in a range of viscosities. The liquid properties are given in Table 1. The density ρ and surface tension σ were measured using an Attension Sigma 702 Force Tensiometer with a standard density probe and Wilhelmy plate, respectively, while the dynamic viscosity μ was provided by the manufacturer and confirmed with an Anton Paar MCR 302 rheometer.

Suspensions were prepared using polystyrene particles of density $\rho = 1050$ kg/m^3 with diameter $2a = 314 \pm 30$ μm, 452 ± 115 μm, 803 ± 92 μm, 897 ± 257 μm, measured using an optical microscope. These particles naturally sink in silicone oils due to a density mismatch with

Table 1
Liquid properties including density ρ, surface tension σ, and dynamic viscosity μ.

Fluids	Density kg/m^3	Surface Tension mN/m	Dynamic viscosity mPa s
10 cSt Si Oil	963.3	19.1 ± 0.8	9.6
20 cSt Si Oil	949.5	19.4 ± 0.7	19
50 cSt Si Oil	957.6	19.5 ± 0.5	47.9
100 cSt Si Oil	959.1	19.4 ± 0.5	95.9
200 cSt Si Oil	965.3	19.4 ± 0.8	193
350 cSt Si Oil	967.1	19.5 ± 0.6	338.5
500 cSt Si Oil	968.7	19.4 ± 0.5	484
1,000 cSt Si Oil	967.7	19.5 ± 0.6	967
5,000 cSt Si Oil	975.1	19.5 ± 0.5	4875
10,000 cSt Si Oil	982.8	19.5 ± 0.7	9828

settling velocity

$$v = \frac{2}{9}\frac{\rho_f \Delta\rho g a^2}{\mu}. \tag{5}$$

The density difference $\Delta\rho = \rho_p - \rho_f$ is small in all our experiments such that the settling velocity V is negligible compared to the substrate velocity U [34]. The particle volume fraction ϕ is

$$\phi = \frac{V_p}{V_p + V_f} \tag{6}$$

where V_p and V_f are the volume of particles and volume of fluid in the suspension, respectively. We restrict our experiments to dilute suspensions ($\phi < 0.005$) to avoid affecting the fluid rheology [20,35].

To begin each experiment, the liquid or suspension was poured into an acrylic container (56 × 26 mm), as shown in Fig. 2(a). Suspensions were stirred until the particles appeared homogeneous. The substrate was lowered until the lower section of the substrate was submerged and then the scale was set to zero. Next, the substrate was lowered 50 mm, then raised 50 mm at a predetermined U and the mass m was recorded. The coating thickness h_0 was computed using gravimetry from the mass m of liquid coating the substrate. Here, h_0 is given by

$$h_0 = \frac{m_t}{\rho A} \tag{7}$$

where A is the surface area of the coated substrate (front and back). Lastly, an image of the coated surface was recorded and later analyzed in ImageJ to determine the size of all entrained particles.

3. Results

Our experimental results on dip coating can be decomposed according to the working liquid and include (i) pure liquid coating, (ii) single particle filtration of monodisperse suspensions, and (iii) particle sorting of bidisperse suspensions.

3.1. Verification of LLD law using pure liquids

Before conducting dip coating experiments of highly viscous suspensions, we verified our experimental setup by reproducing the classic LLD law for completely-wetting liquids. In Fig. 3 we plot the measured coating thickness h_0 against the capillary number Ca (over three decades of data) for silicone oils with viscosity ranging from 47.9 to 9828 mPa·s. We see excellent agreement between our experimental data and the LLD law for all liquids tested. However, we do observe a slight deviation from the LLD law for $Ca > 0.1$, where the effect of gravity-driven drainage becomes considerable. These results demonstrate the reliability of our experimental protocol and give us confidence in the data we report herein.

3.2. Particle filtration of monodisperse suspensions

For a monodisperse suspension, it has been shown that particles can become entrained in the liquid coating film for a range of velocities U [8]. Fig. 4(a) plots the minimum substrate velocity U for entrainment

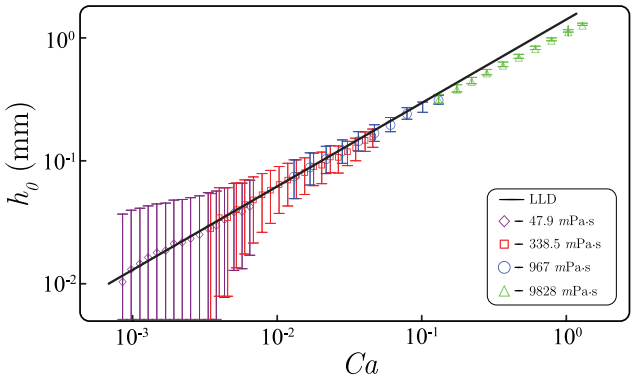

Fig. 3. Coating thickness h_0 against capillary number Ca for pure liquids as it depends upon viscosity with the Landau–Levich–Derjaguin (LLD) law as a solid line.

of a single particle of radius a as it depends on viscosity μ. Lower velocities will not entrain single particles. Here our experimental data for higher viscosity and larger particle sizes are represented by black triangles, while the data from Sauret et al. [8] is indicated by blue squares, red circles, and green diamonds. Here all the data shows that the minimum single particle entrainment velocity U increases monotonically with particle size a and decreases with viscosity μ. For fixed particle size, higher withdrawal velocities are required for less viscous liquids to create a thick enough film to entrain particles.

We can nondimensionalize our data using the capillary number Ca and the Bond number $Bo = (a/\ell_c)^2$ and compare against predictions of the critical capillary number Ca^* given in Eq. (3). Fig. 4(b) plots Ca^* against Bo, with the critical capillary threshold (CCT) from Eq. (3) with best fit prefactor $D = 0.21$ overlaid. Our experimental data agree well with the predicted threshold, indicating that this model is appropriate for larger particle sizes and higher viscosities than previously documented [6,8].

3.3. Sorting of bidisperse suspensions

For a bidisperse suspension made of a small particle with radius a_s and large particle with radius a_l, it is possible to entrain the small particles but not the large particles in an active filtration range of Ca. We perform experiments using three separate bidisperse suspensions of highly viscous liquids. In Fig. 5, we plot the measured particle diameter normalized with the average diameter of the small particle batch a/a_S against the capillary number Ca and highlight three regions: (i) liquid only (white), (ii) active filtration of small particles (striped), and (iii) entrainment of both small and large particles (light gray). We have also included a black dashed box representing the predicted active filtration region as calculated using Eq. (4) using the average diameter for the small and large particles.

Fig. 5 shows the normalized particle diameter against Ca for the different bidisperse suspensions. The entrainment behavior for each suspension is summarized as follows: (a) for $2a$ = 803 μm and $2a$ =

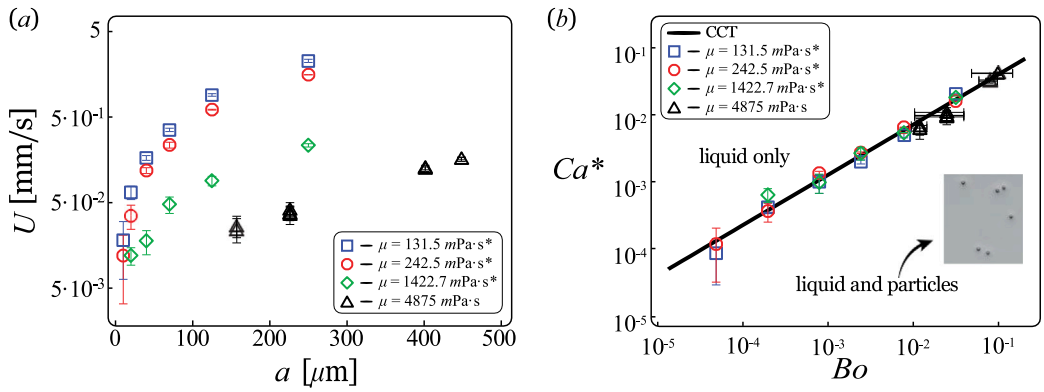

Fig. 4. Particle filtration of monodisperse suspensions. (*a*) Minimum withdrawal velocity U against particle radius a and (*b*) capillary number Ca^* against Bond number Bo for four different liquid viscosities μ. The solid line represents the critical capillary threshold (CCT) $Ca^* = 0.21Bo^{3/4}$ and * denotes data from Sauret et al. [8].

314 μm, no particles are entrained in the coating for $Ca < 7 \times 10^{-3}$, only small particles are entrained for $7 \times 10^{-3} \leq Ca \leq 3.5 \times 10^{-2}$, and both particle sizes are entrained for $Ca > 3.5 \times 10^{-2}$; (b) for $2a = 897$ μm and $2a = 314$ μm, no particles are entrained in the coating for $Ca < 7.5 \times 10^{-3}$, only small particles are entrained for $7.5 \times 10^{-3} \leq Ca \leq 3.5 \times 10^{-2}$, and both particle sizes were entrained for $Ca > 3.5 \times 10^{-2}$; (c) for $2a = 897$ μm and $2a = 803$ μm, no particles are entrained in the coating for $Ca < 3.5 \times 10^{-2}$, only small particles are entrained for $3.5 \times 10^{-2} \leq Ca \leq 5.5 \times 10^{-2}$, and both particle sizes are entrained for $Ca > 5.5 \times 10^{-2}$. Our data show good agreement with the predicted active filtration range from Eq. (4); however, the values that bookend the active filtration region, Ca_B and Ca_S, were slightly lower than predicted. We also note slight inconsistencies in the critical Ca for entrainment of each particle, which is expected but particularly noticeable for our largest particle $2a = 897$ μm—the larger standard deviation of this particle's average diameter explains this variability.

Our results, along with those of Dincau et al. [6], are presented in Fig. 6 as a dimensionless plot of Bo versus Ca. The symbols represent bidisperse suspensions where the small and big particles are denoted by two symbols of the same color and shape. The black line denotes the critical capillary threshold, and the lower and left edges of the plot show the range of Ca for active filtration in suspensions with a particle size difference ΔBo. The color of the bar indicates the associated plot markers. We observe a positive correlation between Bo and Ca with slight deviations from the predicted critical capillary threshold as Ca decreases. The inset of the figure plots ΔBo versus ΔCa on a linear scale, indicating that the capillary range for active filtration increases slower as Bo increases, in qualitative agreement with Eq. (4).

4. Discussion

In this experimental work, we investigated particle entrainment of suspensions using the dip coating process. Our results for particle entrainment of monodisperse suspensions agree with previous reports of three distinct regimes [6,8]. We found that the single particle entrainment points in Fig. 4(*b*) are in good agreement with Eq. (3) with a prefactor of 0.21, which is similar to than predicted by Dincau et al. [6] but differs from the numerical simulations of Colosqui et al. [7]. The variability in prefactors may be attributed to differences in fluid properties, such as surface tension, or variability in particle sizes, which could alter the particle entrainment threshold. This may explain the slight discrepancy between our results and those of Sauret et al. [8], but the larger difference with Colosqui et al. [7] remains unexplained.

Bi-disperse suspensions exhibit three entrainment regimes (i) liquid only, (ii) small particle only, and (iii) both-sized particles. Region (ii), where only the small particles are entrained is the range of active filtration. Our results for the range of active filtration match well with the entrainment model proposed by Sauret et al. [8] but for lower Ca than that predicted (cf. Fig. 5). The cause of this shift is unknown, but considering the standard deviation of the polystyrene particles and fluid properties, the range of active filtration falls within that predicted. Dip coating provides many advantages compared to traditional filtration techniques but can be limited in its range of active filtration (ΔCa) because of equipment limitations (range of U achievable). Interestingly, in the inset of Fig. 6, we show that the active filtration range ΔCa increases more slowly than ΔBo, enabling the sorting of suspensions composed of particles with large Bo differences without requiring significant differences in Ca (U).

Our study fills a critical gap in the existing literature as granular matter ($2a > 100$ μm) is often prevalent in industrial applications, highly viscous liquids play vital roles in industrial and biological applications, and their combination produces suspensions that require a dependable method for filtering and sorting their components. Nonetheless, numerous unanswered questions remain. The range of fluid properties yet to be explored is vast and this includes fluids with complex rheologies. Shear-thinning liquids are particularly interesting since many coatings, like paints, rely on knowing the critical substrate velocity to prevent contaminating the coating. Recently, Bertin et al. [36] proposed a model for dip coating of soft substrates, indicating a new scaling relationship for the coating thickness and an elastocapillary region where the substrate and liquid–air interface are curved. Therefore, the process of particle entrainment will likely differ for a soft substrate being pulled from a bath and could help us understand particle entrainment on soft biological substrates, such as a tongue. Alternatively, suppose the particles or both the substrate and particles are soft materials. In that case, the particle entrainment process may exhibit new physics that can aid our comprehension of fluid flow phenomena and soft matter physics.

5. Conclusions

We conducted dip coating experiments for granular suspensions of highly viscous silicone oils. Our observations for monodisperse suspensions were consistent with prior investigations [8], and we observed the same qualitative regimes of liquid-only, clumps, and single particle entrainment. Furthermore, we could predict single particle entrainment using Eq. (3) for higher viscosity liquids and larger particles than previously explored, thus filling a critical gap in the literature. We demonstrate that dip coating of bidisperse suspensions can be used as a means for active filtration for Bo and Ca an order of magnitude greater than previously explored. Lastly, we compare the Ca filtration range for each range of Bo and show that the range of particle sizes (Bo) exhibits a greater increase than Ca, allowing for large particle size differences (ΔBo) to be filtered without having to drastically increase the range of Ca that the coating system can achieve during operation.

Our results provide new empirical data and validation of particle entrainment models for variable ranges not previously explored. These

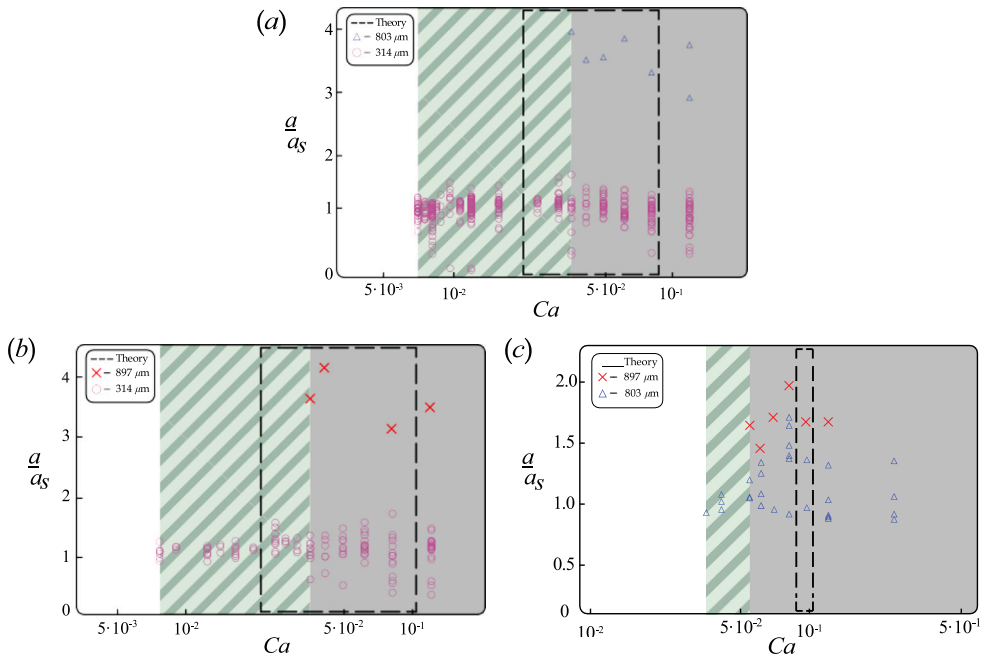

Fig. 5. Particle sorting of bidisperse suspensions by plotting the normalized size a/a_s of entrained particles, where a_s is the radius of the smaller particle in the suspension, against the capillary number Ca, for bidisperse suspensions of (*a*) 314 μm and 803 μm, (*b*) 314 μm and 897 μm, and (*c*) 803 μm and 897 μm particles in silicone oil with viscosity $\mu = 4875$ mPa s. The plot shading indicates the Ca range where no particles (unshaded), small particles (striped), and both particles (gray) are entrained by the liquid film. The dashed box indicates the predicted active filtration region from $Ca^* = 0.21\,Bo^{3/4}$.

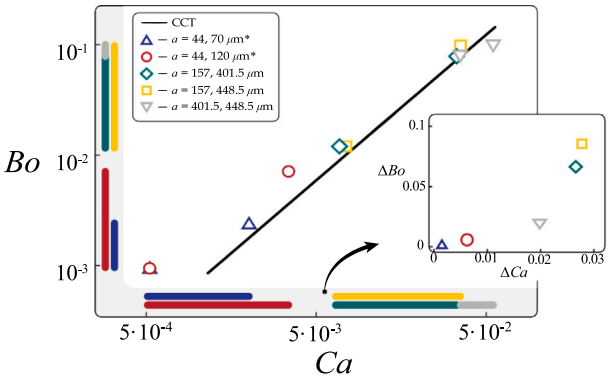

Fig. 6. Non-dimensional particle sorting of bidisperse suspensions. Bond number Bo plotted against capillary number Ca for different particle size combinations. Each color-symbol combination has two data markers corresponding to the entrainment point of the smallest particle (lower marker) and largest particle. The range of Bo and Ca for each experiment is shown by the colored bars along the plot's lower and left edge and plotted in the inset. An * indicates data from Dincau et al. [6].

variable ranges are expanded for monodisperse particle filtering but especially for bidisperse sorting. Previous research on bidisperse sorting explored suspensions with particles of diameter $88 \leq 2a \leq 240$ μm and silicone oil with a viscosity $\mu = 132$ mPa · s [6]. Here, we explored particle sorting for suspensions with larger particle diameter $314 \leq 2a \leq 897$ μm and highly viscous silicone oil $\mu = 4875$ mPa · s, giving us access to a critical parameter space for many applications, as discussed in detail earlier. The number of potential uses for capillary filtration and sorting is vast and growing as the global market for microspheres reached 3.8 billion USD in 2021 and is projected to surpass 5 billion USD by 2027 [37]. The development of novel functional microsphere suspensions contribute greatly to these estimates. For example, several smart coating technologies are being developed with advanced chemical properties, corrosion protection, and self-healing properties [38–40]. Sustainable microspheres [41] and biosensors [42] that can be used for these suspensions can reach up to 500 and 300 μm, respectively, and may be considered granular suspensions. In culinary product production, suspended granular media in viscous liquid is abundant and includes propolis in honey, peanut pieces in peanut butter, and the aroma microspheres with diameters around 450 μm developed by flavor engineers [43,44]. Thus, the physics of particle sorting in viscous suspensions can help achieve the desired particle distribution in culinary products and may also govern the flavors experienced when eating a flavor-engineered sauce. Many aspects of such applications are yet to be explored, such as particle sorting on an elastic substrate (like the human tongue), but our work has expanded the study of bidisperse sorting and particle filtration and opens the door for interesting future topics, particularly at the intersection of fluid mechanics and soft matter physics where many practical phenomena occur.

CRediT authorship contribution statement

Connor Copeland: Methodology, Verification, Investigation, Formal analysis, Visualization, Writing – original draft. **Chase T. Gabbard:** Investigation, Formal analysis, Visualization, Writing – original draft. **Joshua B. Bostwick:** Conceptualization, Writing – review & editing, Supervision, Funding acquisition.

Declaration of competing interest

The authors declare the following financial interests/personal relationships which may be considered as potential competing interests: Joshua Bostwick reports financial support was provided by National Science Foundation.

Data availability

Data will be made available on request.

Acknowledgment

JBB acknowledges support from NSF Grant CBET-1750208.

References

[1] B. Levich, L. Landau, Dragging of a liquid by a moving plate, Acta Physicochim. URSS 17 (1942) 42.
[2] B.V. Deriagin, S.M. Levi, Film Coating Theory: The Physical Chemistry of Coating Thin Layers on a Moving Support, Focal Press, 1964.
[3] E. Rio, F. Boulogne, Withdrawing a solid from a bath: How much liquid is coated? Adv. Colloid Interface Sci. 247 (2017) 100–114.
[4] P. Baumeister, Optical Coating Technology, vol. 137, SPIE Press, 2004.
[5] C. Crowe, M. Sommerfeld, Y. Tsuji, et al., Multiphase flows with, Ž, 1998.
[6] B.M. Dincau, M.Z. Bazant, E. Dressaire, A. Sauret, Capillary sorting of particles by dip coating, Phys. Rev. A 12 (2019) 011001.
[7] C.E. Colosqui, J.F. Morris, H.A. Stone, Hydrodynamically driven colloidal assembly in dip coating, Phys. Rev. Lett. 110 (2013) 188302.
[8] A. Sauret, A. Gans, B. Colnet, G. Saingier, M.Z. Bazant, E. Dressaire, Capillary filtering of particles during dip coating, Phys. Rev. Fluids 4 (2019) 054303.
[9] Z. Xu, Filtration mechanism of fine particle, in: Fundamentals of Air Cleaning Technology and Its Application in Cleanrooms, Springer, 2014, pp. 133–183.
[10] B. Derjaguin, On the thickness of the liquid film adhering to the walls of a vessel after emptying, Progress Surf. Sci. 43 (1993) 134–137.
[11] A. De Ryck, D. Quéré, Gravity and inertia effects in plate coating, J. Colloid Interface Sci. 203 (1998) 278–285.
[12] F. Goucher, H. Ward, A problem in viscosity, Phil. Mag. 44 (1922) 1002.
[13] M. Maleki, M. Reyssat, F. Restagno, D. Quéré, C. Clanet, Landau–Levich menisci, J. Colloid Interface Sci. 354 (2011) 359–363.
[14] J.A. Tallmadge, Withdrawal of flat plates from power law fluids, AIChE J. 16 (1970) 925–930.
[15] R. Spiers, C. Subbaraman, W. Wilkinson, Free coating of non-Newtonian liquids onto a vertical surface, Chem. Eng. Sci. 30 (1975) 379–395.
[16] J. Snoeijer, J. Ziegler, B. Andreotti, M. Fermigier, J. Eggers, Thick films of viscous fluid coating a plate withdrawn from a liquid reservoir, Phys. Rev. Lett. 100 (2008) 244502.
[17] R. Krechetnikov, G. Homsy, Experimental study of substrate roughness and surfactant effects on the Landau-Levich law, Phys. Fluids 17 (2005) 102108.
[18] D.M. Campana, S. Ubal, M.D. Giavedoni, F.A. Saita, Influence of surfactants on dip coating of fibers: Numerical analysis, Ind. Eng. Chem. Res. 55 (2016) 5770–5779.
[19] A.Q. Shen, B. Gleason, G.H. McKinley, H.A. Stone, Fiber coating with surfactant solutions, Phys. Fluids 14 (2002) 4055–4068.
[20] B.M. Dincau, E. Mai, Q. Magdelaine, J. Lee, M. Bazant, A. Sauret, Entrainment of particles during the withdrawal of a fibre from a dilute suspension, J. Fluid Mech. 903 (2020).
[21] D.-H. Jeong, A. Kvasnickova, J.-B. Boutin, D. Cébron, A. Sauret, Deposition of a particle-laden film on the inner wall of a tube, Phys. Rev. Fluids 5 (2020) 114004.
[22] T. Wu, Z. Yang, R. Hu, Y.-F. Chen, H. Zhong, L. Yang, W. Jin, Film entrainment and microplastic particles retention during gas invasion in suspension-filled microchannels, Water Res. 194 (2021) 116919.
[23] D.-H. Jeong, L. Xing, J.-B. Boutin, A. Sauret, Particulate suspension coating of capillary tubes, Soft Matter 18 (2022) 8124–8133.
[24] Y.E. Yu, S. Khodaparast, H.A. Stone, Separation of particles by size from a suspension using the motion of a confined bubble, Appl. Phys. Lett. 112 (2018) 181604.
[25] D.-H. Jeong, M.K.H. Lee, V. Thiévenaz, M.Z. Bazant, A. Sauret, Dip coating of bidisperse particulate suspensions, J. Fluid Mech. 936 (2022) A36.
[26] J. Amirian, P. Makkar, G.H. Lee, K. Paul, B.T. Lee, Incorporation of alginate-hyaluronic acid microbeads in injectable calcium phosphate cement for improved bone regeneration, Mater. Lett. 272 (2020) 127830.
[27] K. Saralidze, L.H. Koole, M.L. Knetsch, Polymeric microspheres for medical applications, Materials 3 (2010) 3537–3564.
[28] J.S. How, C.T. Young, Factors affecting peanut butter preference, J. Am. Oil Chem. Soc. 62 (1985) 538–540.
[29] A.O. Oyedele, et al., Fluid emulsion base potential of shea butter, J. Pharmacy Bioresour. 13 (2016) 103–113.
[30] M.-S. Kwak, H.-J. Ahn, K.-W. Song, Rheological investigation of body cream and body lotion in actual application conditions, Korea-Aust. Rheol. J. 27 (2015) 241–251.
[31] N. Hasan, D.R.A. Biak, S. Kamarudin, Application of bacterial cellulose (bc) in natural facial scrub, Int. J. Adv. Sci. Eng. Inf. Technol. 2 (2012) 272.
[32] J. Kitsongsermthon, K. Duangweang, J. Kreepoke, A. Tansirikongkol, In vivo cleansing efficacy of biodegradable exfoliating beads assessed by skin bioengineering techniques, Skin Res. Technol. 23 (2017) 525–530.
[33] N. Xue, H.A. Stone, Self-similar draining near a vertical edge, Phys. Rev. Lett. 125 (2020) 064502.
[34] H. Lamb, Hydrodynamics, University Press, 1924.
[35] P.S. Raux, A. Troger, P. Jop, A. Sauret, Spreading and fragmentation of particle-laden liquid sheets, Phys. Rev. Fluids 5 (2020) 044004.
[36] V. Bertin, J.H. Snoeijer, E. Raphaël, T. Salez, Enhanced dip coating on a soft substrate, Phys. Rev. Fluids 7 (2022) L102002.
[37] B. Research, Microspheres: Technologies and Global Markets, BCC Research, Wellesley, 2022.
[38] Y. Zhu, M. Chen, L. Wu, Synthesis of uv-responsive dual-functional microspheres for highly efficient self-healing coatings, Chem. Eng. J. 422 (2021) 130034.
[39] X. Ni, Y. Gao, X. Zhang, Y. Lei, G. Sun, B. You, An eco-friendly smart self-healing coating with nir and ph dual-responsive superhydrophobic properties based on biomimetic stimuli-responsive mesoporous polydopamine microspheres, Chem. Eng. J. 406 (2021) 126725.
[40] J. Gao, X. Huang, H. Xue, L. Tang, R.K. Li, Facile preparation of hybrid microspheres for super-hydrophobic coating and oil-water separation, Chem. Eng. J. 326 (2017) 443–453.
[41] C.A. King, J.L. Shamshina, O. Zavgorodnya, T. Cutfield, L.E. Block, R.D. Rogers, Porous chitin microbeads for more sustainable cosmetics, ACS Sustain. Chem. Eng. 5 (2017) 11660–11667.
[42] H. Zhu, J.D. Suter, I.M. White, X. Fan, Aptamer based microsphere biosensor for thrombin detection, Sensors 6 (2006) 785–795.
[43] V. Manojlovic, N. Rajic, J. Djonlagic, B. Obradovic, V. Nedovic, B. Bugarski, Application of electrostatic extrusion – flavour encapsulation and controlled release, Sensors 8 (2008) 1488–1496, http://dx.doi.org/10.3390/s8031488.
[44] J. Uhlemann, B. Schleifenbaum, H.-J. Bertram, Flavor encapsulation technologies: An overview including recent developments, Perfumer Flavorist 27 (2002) 52–61.